Hollow microgels squeezed in overcrowded environments

A. Scotti, M. Brugnoni, A. A. Rudov, J. E. Houston, I. I. Potemkin, and W. Richtering

Citation: The Journal of Chemical Physics **148**, 174903 (2018); doi: 10.1063/1.5026100
View online: https://doi.org/10.1063/1.5026100
View Table of Contents: http://aip.scitation.org/toc/jcp/148/17
Published by the American Institute of Physics

Hollow microgels squeezed in overcrowded environments

A. Scotti,[1,a)] M. Brugnoni,[1] A. A. Rudov,[2,3] J. E. Houston,[4] I. I. Potemkin,[2,3,5] and W. Richtering[1,6,b)]

[1]*Institute of Physical Chemistry, RWTH Aachen University, 52056 Aachen, Germany*
[2]*Physics Department, Lomonosov Moscow State University, 119991 Moscow, Russian Federation*
[3]*DWI–Leibniz Institute for Interactive Materials e.V., Aachen 52056, Germany*
[4]*Jülich Centre for Neutron Science (JCNS) at Heinz Maier-Leibnitz Zentrum (MLZ), Forschungszentrum Jülich GmbH, Lichtenbergstr. 1, 85748 Garching, Germany*
[5]*National Research South Ural State University, Chelyabinsk 454080, Russian Federation*
[6]*JARA-SOFT, 52056 Aachen, Germany*

(Received 15 February 2018; accepted 16 April 2018; published online 3 May 2018)

We study how a cavity changes the response of hollow microgels with respect to regular ones in overcrowded environments. The structural changes of hollow poly(*N*-isopropylacrylamide) microgels embedded within a matrix of regular ones are probed by small-angle neutron scattering with contrast variation. The form factors of the microgels at increasing compressions are directly measured. The decrease of the cavity size with increasing concentration shows that the hollow microgels have an alternative way with respect to regular cross-linked ones to respond to the squeezing due to their neighbors. The structural changes under compression are supported by the radial density profiles obtained with computer simulations. The presence of the cavity offers to the polymer network the possibility to expand toward the center of the microgels in response to the overcrowded environment. Furthermore, upon increasing compression, a two step transition occurs: First the microgels are compressed but the internal structure is unchanged; then, further compression causes the fuzzy shell to collapse completely and reduce the size of the cavity. Computer simulations also allow studying higher compression degrees than in the experiments leading to the microgel's faceting. *Published by AIP Publishing.* https://doi.org/10.1063/1.5026100

I. INTRODUCTION

In recent years, many advances have been achieved in the design of microgels with different internal structures. In addition to the usual thermo-responsive microgels that can be modeled as fuzzy spheres (Fig. 1, top),[1] both core-shell[2–4] and hollow shell microgels[5–7] have been successfully synthesized. The former have a rigid, incompressible core surrounded by a polymeric network, while the latter present a solvent filled cavity surrounded by a fuzzy shell.[7–9]

Hollow microgels represent an appealing model system for the advance in the tailoring of nanocapsules for drug delivery.[10–12] Furthermore, thin films of such microgels can be successfully used to realize membranes for water filtration.[13] It has been shown that the absence of a rigid core strongly affects the behavior of a 2D suspension under compression leading to a more pronounced deformation of the hollow microgels.[14] Their unique internal structure and the capability to tune their size depending on external stimuli, e.g., temperature,[7–9,15] make these microgels versatile for various applications.[16]

The absence of a rigid core makes hollow microgels an ideal system to investigate the effect of their internal structure on the equilibrium phase behavior of the suspension. The fuzzy shell is the soft, outer part of the microgels, which determines the interaction between them. Recently, it has been shown that the presence of the soft compressible corona has an effect on the crystallization of soft spheres[17,18] or star polymers[19] in suspension.

For typical cross-linked microgels synthesized via precipitation polymerization, the compression of the fuzzy corona has previously been probed (Fig. 1, deswelling) with small-angle neutron scattering (SANS).[20] However, interpenetration between microgels above the random close packing has been observed as well (Fig. 1, interpenetration).[21] The prevalence of deswelling with respect to interpenetration between the microgels (and vice versa) depends both on the relative softness of the microgels in suspensions and their internal structure and cross-linker distribution.[22] Furthermore, larger microgels studied with microscopy showed significant faceting and deformation (Fig. 1, deformation).[22,23] More detailed studies are needed to investigate the behavior of soft microgels in concentrated suspensions and relate their properties with other soft colloids, for instance star polymers.[24]

Furthermore, hollow microgels do not have a corresponding "atomic" counterpart, but rather a cavity in their internal structure which makes them different from the usual hard or soft spheres used to reproduce and study the behavior of atomic systems.[25–28] They represent a new kind of system that can show distinguishable and unexplored properties with

[a)]scotti@pc.rwth-aachen.de
[b)]richtering@rwth-aachen.de

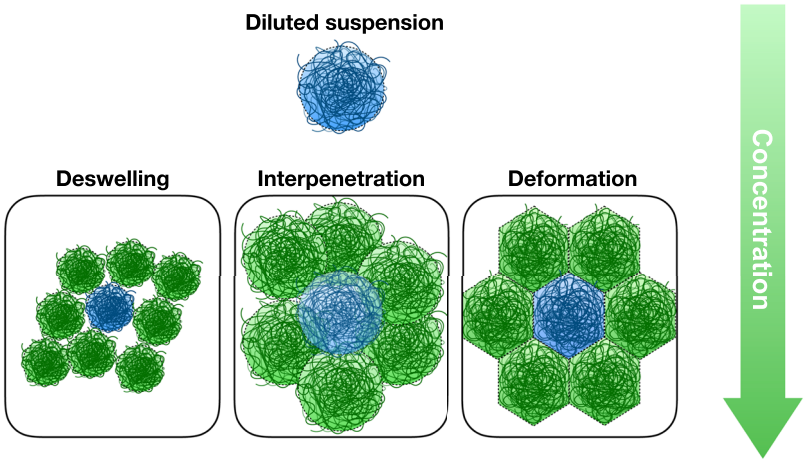

FIG. 1. Possible responses of a microgel (blue) to the increase of concentrations: isotropic deswelling (bottom left); interpenetration (bottom central); and deformation with faceting (bottom right).

respect to colloidal suspensions. New features of these microgels can arise from their unique internal structure. This means they will differ from the usual colloidal suspensions both in concentrated environments and in the swelling/deswelling behavior.

To understand whether a cavity changes the response of a polymer network under compression, we have measured the form factors of few hollow microgels in concentrated suspensions of regular microgels using SANS with contrast variation. The poly(*N*-isopropylacrylamide) (pNIPAM) hollow microgels are dispersed in a matrix of deuterated regular microgels synthesized using deuterated NIPAM ($C_6D_7H_4NO$, D7-NIPAM) and the same amount of cross-linker (5 mol. %). The latter are then contrast matched with a mixture of water/heavy water. Therefore, the form factors of the hollow microgels are directly measured at different concentrations. By fitting the scattering intensities with a model developed for hollow spheres, the radial distribution of the polymer inside the microgels is obtained.[7]

Computer simulations reproducing the experimental conditions have been conducted to compare their results to the experimental radial profiles and to probe the compression of the neighbors of the hollow microgels. The data show that with increasing microgel concentration in the suspension, first the microgels are compressed without significant changes in the internal structure. Then, a stronger decrease of the size of the microgel is observed. In this stage, the polymeric chains expand within the cavity and the fuzzy shell is completely collapsed. This mechanism is due to the presence of the internal cavity and offers an alternative way to respond to the increased concentration of microgels in the suspension.

II. EXPERIMENTAL

A. Synthesis

The synthesis of hollow microgels relies on the generation of silica-core pNIPAM-shell microgels with subsequent core dissolution. The sacrificial silica cores were obtained by the well-known *Stöber* synthesis.[29] Ethanol (700 ml) was heated under reflux to 60 °C. Ammonia solution (80 ml 28%-32%) was added and after 10 min of equilibration time, the reaction was started by adding 25 ml tetraethyl orthosilicate (TEOS). After 24 h, the particles were surface modified using 3-methacryloxypropyltrimethoxysilane (MPS) as previously reported.[15] The silica cores were purified by threefold centrifugation at 5000 rpm and redispersion in fresh ethanol. For storage, the solvent was evaporated.

The core-shell synthesis was performed by dispersing 1.5 g silica cores in 10 ml ethanol. The suspension was sonicated to prevent from silica aggregates during the shell polymerization. Subsequently, it was transferred to a monomer solution of 0.7960 g NIPAM ($C_6H_{11}NO$), 57.3 mg *N*,*N*′-methylenebisacrylamide (BIS), and 116.0 mg sodium dodecyl sulfate (SDS) in 195 ml filtered (0.2 μm regenerate cellulose membrane filter) double-distilled water. SDS was used to minimize the size polydispersity.[30] The solution was purged with nitrogen under stirring at 200 rpm and heated to 60 °C. Simultaneously, a solution of 84.0 g potassium peroxydisulfate (KPS) in 5 ml filtered double-distilled water was degassed. To start the polymerization, the initiator solution was rapidly transferred to the monomer solution. The reaction was left to proceed for 4 h under constant nitrogen flow and stirring at 60 °C. The core-shell microgels were purified by threefold ultra-centrifugation at 30 000 rpm and redispersion in fresh water. Lyophilization was performed for storage.

To generate hollow microgels, the silica cores were dissolved by means of a sodium hydroxide (NaOH) solution.[8] Briefly, 1.100 g core-shell microgels were redispersed in 50 ml water. After complete dispersion, 50 ml 0.1 M NaOH solution was added and left to react for 4 days. Dialysis was applied to remove the remaining silica and neutralize the suspension. Finally, the resulting hollow microgels were centrifuged at 50 000 rpm to reduce the total volume and lyophilization was carried out for storage.

The polymerization of the deuterated microgels was performed by dissolving 1.4280 g D7-NIPAM ($C_6D_7H_4NO$), 96.4 mg BIS, and 19.2 mg SDS in 80 ml filtered double-distilled water. The suspension was degassed by purging with nitrogen under stirring at 200 rpm and 60 °C. Simultaneously, the initiator solution of 35.2 mg KPS in 5 ml water was degassed. The polymerization was initiated by transferring the initiator solution rapidly to the monomer solution. The reaction was left to proceed for 4 h.

Ultra-centrifugation and lyophilization were used for purification and storage.

B. Dynamic light scattering

Both the deuterated and the hollow microgels were characterized with dynamic light scattering (DLS). An instrument equipped with a laser with wavelength in vacuum $\lambda_0 = 633$ nm and an index matched thermal bath filled with toluene was used. Suspensions of diluted microgels in water (or heavy water), with refractive index $n = 1.33$, were measured. The scattering vector, $q = (4\pi n)/\lambda_0 \sin(\theta/2)$, was changed by varying the scattering angle, θ, between 30° and 110° with steps of 10°. The swollen state of the microgels was determined at a temperature, T, equal to (20.00 ± 0.01) °C. The microgels were dispersed in pure heavy water to allow for a direct comparison with the form factor measured with small-angle neutron scattering. This is done since both the swelling[31] and the volume phase transition temperature (VPTT)[32] of pNIPAM are different in heavy water with respect to regular water. The swelling behavior in pure double-distilled water is shown in Fig. S1 of the supplementary material.

The intensity autocorrelation functions were analyzed with second cumulant analysis[33] to obtain the decay rates, Γ, for each q. Since the average diffusion coefficient, D_0, is linked to the decay rate by the relation $\Gamma = q^2 D_0$, a linear fit led to the value of D_0.[34] Finally, the hydrodynamic radius was computed using the Stokes-Einstein equation: $R_h = k_b T/(6\pi\eta D_0)$ where k_b and $\eta = 1.25$ mPa·s[35] are the Boltzmann constant and the viscosity of heavy water at (20.00 ± 0.01) °C, respectively. The hydrodynamic radius for the hollow microgels was (211 ± 3) nm while that of the deuterated microgels was (227 ± 2) nm. The size distributions of the suspended microgels were obtained from the CONTIN[36,37] analysis of the intensity autocorrelation functions with a modified algorithm.[38] The size polydispersities for the hollow and deuterated microgels were (11 ± 4)% and (10 ± 2)%, respectively.

C. Small-angle neutron scattering

Small-angle neutron scattering experiments were performed at the KWS-2 instrument operated by JCNS at the Heinz Maier-Leibnitz Zentrum (MLZ), Garching, Germany. Three configurations were used to cover the q-range of interest: Sample detector distance, $d_{SD} = 20$ m with neutron wavelength $\lambda = 10$ Å, $d_{SD} = 8$ m with $\lambda = 5$ Å, and $d_{SD} = 2$ m with $\lambda = 5$ Å. Due to the velocity selector, the resolution in lambda was 20%. The instrument was equipped with a ^{3}He detector with a pixel size <8 mm.

For all the samples, the concentration of the hollow microgels was kept low. In this way, the structure factor of these microgels was approximated to one. Furthermore, as shown in the supplementary material, a solvent composed of 90 wt. % of heavy water, in a heavy water/water mixture, matches the scattering length density of the deuterated, regular microgels, which as a result were "invisible" during the experiments. Therefore, the scattered intensity, $I(q)$, was directly proportional to the form factor of the hollow microgels, $P(q)$, that contains information about their shape and the internal structure. All the measurements were performed at a fixed temperature equal to (20.0 ± 0.5) °C. To probe the collapsed state of the microgels, the form factor was acquired at T = (40.0 ± 0.5) °C, well above the VPTT of pNIPAM.[32,39]

D. Molecular dynamics simulations

The regular (continuous) and hollow microgels were designed in a similar way as reported in the literature.[14,40,41] Fully stretched subchains (arrays of identical beads, each of the radius σ and mass m, equidistantly located from each other) of the same length were arranged and connected through tetrafunctional cross-linkers to form a modified diamond unit cell. The positions of cross-linkers in the constructed cell repeat the pattern of a diamond cubic crystal structure. 15 × 15 × 15 modified unit cells (a frame) of the subchain length of 10 beads have been used to generate microgels with 5% of cross-links. To get the spherical microgel, a sphere is inscribed into the frame. All the beads, which are outside the sphere, were cropped out. In the case of the hollow microgel, two concentric spheres are inscribed into the frame. Part of the network between the spheres is retained and all other beads are cropped out; see Fig. S7 of the supplementary material.

To follow the experimental conditions, the radii of both continuous and hollow microgels are chosen to be equal. The radius of the cavity was selected in such a way to keep the ratio between cropped from the cavity and remaining numbers of the beads to be 0.05; see Fig. S7 of the supplementary material.

The LAMMPS package[42] was used to perform the Brownian molecular dynamics simulations within a standard coarse-grained model with implicit solvent. Connectivity of the beads into the polymer network was realized via combining the finite extension nonlinear elastic (FENE)[43] and repulsive Lennard-Jones potentials. The latter describes repulsion between the beads. It is quantified by the interaction parameter ε. Parameters of the FENE potential, i.e., the maximum of the bond length, R_0, and spring constant, K, are taken in a standard form,[43] $R_0 = 1.5\sigma$ and $K = 30\varepsilon/\sigma^2$. The interactions between any pair of the beads (solvent quality) were described through the truncated-shifted Lennard-Jones potential.[44] The value of the dimensionless Lennard-Jones interaction parameter ε_{bb} describing bead-bead interactions was set to $\varepsilon_{bb} = 0.1\varepsilon$ and $r_{cut} = 1.5\sigma$. These values of the parameters correspond to the case of a good solvent. The simulations were carried out using dimensionless units of the parameters, $\varepsilon = \sigma = m = 1$. The equations of motion were integrated with a time step $\Delta t = 0.01\tau$, where τ is the standard time unit for a Lennard-Jones fluid.

First, the equilibrium characteristics of all microgels in the dilute solution regime have been found. For this, we placed single microgels into the cubic simulation box of the size $L = L_x = L_y = L_z = 200\sigma$ with imposed periodic boundary conditions. We carried out $10 \cdot 10^6$ equilibration runs and obtained statistics from the next $5 \cdot 10^6$ runs in the NVT ensemble at temperature $T = 1$. The density profiles of the microgels are presented in Fig. S8 of the supplementary material. As expected

from the design conditions, both microgels reveal equal swelling degree and polymer concentration in the network. The hollow microgel has a distinct cavity under good solvent conditions.

To study the structure evolution of the microgels in a densely packed system, which is subjected to compression, the microgels were placed into a cubic simulation box of the size $L = L_x = L_y = L_z = 200\sigma$ and packed with the symmetry of the face-centered cubic (fcc) lattice. They occupied $2 \times 2 \times 2$ unit cells of the lattice parameters $a = b = c = 70.6\sigma$, Fig. 4(a). The total number of the microgels in the simulation box was 32. The red microgel in Fig. 4 is the hollow one, which is embedded within the matrix of regular microgels. Compression of the microgels is simulated with non-equilibrium MD (NEMD) simulations of a continuously strained system.[45,46] During the t_α steps of the deformation run, we changed the volume of the simulation box by simultaneously decreasing L from 200σ to $\alpha \cdot 200\sigma$. The compression degree α was varied from 1 to 0.5 with a step 0.1. To have the same speed of compression for each α, we set $t_\alpha = \frac{1-\alpha}{0.5} t_{\alpha=0.5}$, where $t_{\alpha=0.5} = 10^6$ steps. After each compression, we used the classical MD simulations in the NVT ensemble at temperature $T = 1$ and performed dynamic run for $10 \cdot 10^6$ and obtained statistics from the next $5 \cdot 10^6$ runs.

III. RESULTS AND DISCUSSION

In this work, we want to understand whether the presence of a cavity makes a difference in the deswelling of hollow microgels in an overcrowded environment, in comparison to regular cross-linked microgels synthesized via precipitation polymerization. Different degrees of compression were achieved by increasing the concentration of regular microgels composing the matrix where the hollow ones were embedded. The regular cross-linked microgels were synthesized with the same molar content (5 mol. %) of cross-linker agents used to make hollow microgels. In this way, the stiffness and elasticity of the polymer network were comparable for the two systems. The monomer used to synthesize the regular microgels was deuterated NIPAM, $C_6D_7H_4NO$.

We used deuterated microgels as the matrix since hydrogen and deuterium have a different scattering length density. In small-angle neutron scattering, a proper mixture of water and heavy water can match the signal of the deuterated microgels. This allows us to obtain the form factor of hollow (protonated) microgels in overcrowded environments.[21,47] Furthermore, we used a matrix of regular microgels instead of hollow ones to directly compare our findings with other experiments performed of regular microgels in overcrowded environments.[17,20,21,23] In this way, it is evident whether the presence of the cavity has effects on the compression of the microgels with respect to regular ones, once embedded in a similar matrix.

The concentrations of the samples are expressed by the generalized volume fraction, ζ, that represents the volume occupied by the particles in their swollen state divided by the total available volume in the suspension. In contrast to hard, incompressible spheres, ζ can exceed 0.74, reflecting the possibility of interpenetration,[21,23] the deformability[22,23,48] or the capability to be compressed[20,49] of the soft microgels. The generalized volume fraction is related to the mass concentration of the microgels in the suspension, c, by a conversion constant, k: $\zeta = kc$. The values of k for the hollow (HS) and regular deuterated (D) microgels are obtained using viscosimetry,[20,21,50] k_{HS} and k_D, respectively. This is shown in Fig. S2 of the supplementary material. Using the values of the conversion constants, the generalized volume fractions of both the hollow and the deuterated microgels were computed, ζ_{HS} and ζ_D, respectively. The total volume fraction of the mixture is $\zeta = \zeta_{HS} + \zeta_D$.

A series of samples with ζ between (0.244 ± 0.006) and (1.04 ± 0.03) were prepared. For all suspensions, the concentration of the hollow microgels was $\zeta_{HS} < 0.08$ and, therefore, the interactions between them can be neglected. The solvent for the concentrated suspensions was 90 wt. % heavy water in a water/heavy water mixture. As shown in Fig. S3 of the supplementary material, this solvent matches the scattering length density of the deuterated microgels making them invisible during the experiment. The form factors of the hollow microgels and their changes with increasing the microgel concentration in suspension, i.e., ζ, were directly measured with small-angle neutron scattering.

The data have been fitted using a model proposed by Dubbert *et al.* for core fuzzy shell microgels.[7] Briefly, the parameters of the fit are the size of the internal cavity, R_{cav}, the size of the internal fuzzy shell, $2\sigma_{int}$, the width of a constant concentration area, ws, the width of the external fuzzy shell, $2\sigma_{ext}$, the size polydispersity, σ_p, and the correlation length ξ. Finally the model is convoluted with the resolution of the instrument[51] and a constant background is added to account for the incoherent scattering. An example of the radial distribution of hollow microgels is sketched in Fig. 2. The total radius of the microgel is $R_{HS} = R_{cav} + 2\sigma_{int} + ws + 2\sigma_{ext}$.

To check if the cavity persisted after dissolving the silica core, the form factor of the hollow spheres in a diluted suspension of pure heavy water was measured well below and above the volume phase transition temperature of pNIPAM. The scattering curves at (20.0 ± 0.5) and $(40.0 \pm 0.5)\,^\circ$C,

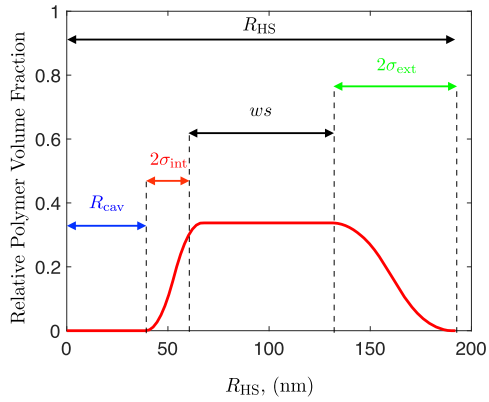

FIG. 2. Sketch of the radial distribution of the relative polymer volume fraction of hollow microgels where the size of the internal cavity, R_{cav}, the width of the internal fuzzy shell, $2\sigma_{int}$, the size of a constant concentration area, ws, and the width of the external fuzzy shell, $2\sigma_{ext}$, are indicated. R_{HS} is the total radius of the microgel.

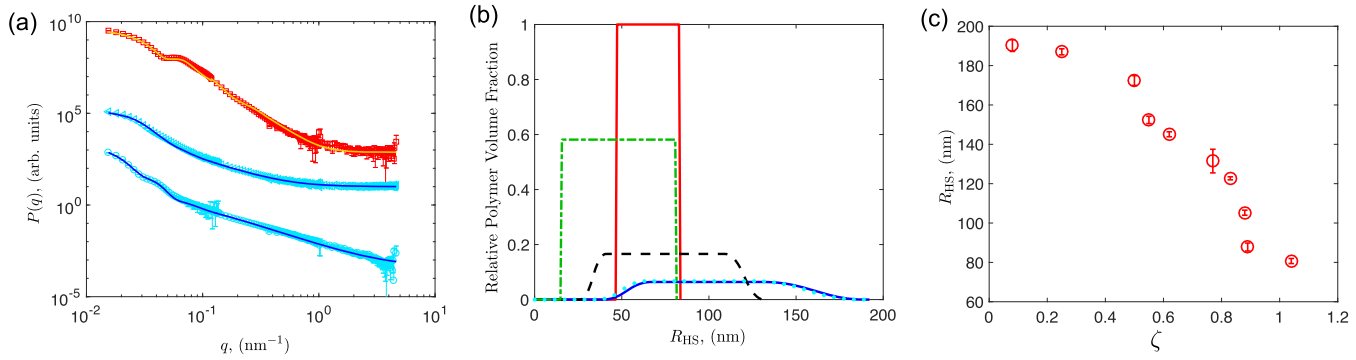

FIG. 3. (a) SANS form factors of the hollow microgels at different total concentrations. Cyan empty circles: (20.0 ± 0.5) °C, ζ = 0.08 ± 0.01 in pure heavy water. Red empty squares: (40.0 ± 0.5) °C, ζ < 0.08 ± 0.01 in pure heavy water. Cyan empty triangles: (20.0 ± 0.5) °C, ζ = 1.04 ± 0.03 in 90 wt. % heavy water in water/heavy water mixture. The solid lines represent the fits with the model described in Ref. 7. The data represented with cyan empty triangles and red empty squares are shifted up for clarity. (b) Relative polymer volume fraction of the hollow microgels: (20.0 ± 0.5) °C and ζ = 0.08 ± 0.01 (solid blue line), (20.0 ± 0.5) °C and (0.244 ± 0.006) (dotted cyan line), (20.0 ± 0.5) °C and ζ = 0.77 ± 0.02 (dashed black line), (20.0 ± 0.5) °C and ζ = 1.04 ± 0.03 (dashed-dotted green line), and (40.0 ± 0.5) °C (solid red line). (c) Radius of the hollow microgel, R_{HS} (red empty circles), versus the generalized volume fraction, ζ, obtained from the fit of the form factors of the hollow microgels measured at different total concentrations [panel (a) and Fig. S5 of the supplementary material].

cyan empty circles and red empty squares, respectively, are plotted in Fig. 3(a). The red empty squares data are shifted in the *y*-direction for clarity. The solid lines represent the fits with the core fuzzy shell model[7,8] to the data.

The relative polymer volume fractions are plotted in Fig. 3(b), the solid blue and red lines for (20.0 ± 0.5) and (40.0 ± 0.5) °C, respectively. All curves were normalized with respect to the polymer volume fraction within the microgel in the collapsed state, red curve in Fig. 3(b), since the amount of polymer composing the microgel remains constant independently of the temperature.

The blue profile shows the microgel in the swollen state. The cavity has a size R_{cav} = (39.1 ± 0.5) nm; then, an increase of the density, in a region with a width $2\sigma_{int}$ = (27.7 ± 0.6) nm, is followed by a region with constant polymer density with a size *ws* = (64 ± 2) nm. After this, the concentration of the polymer decays in the external fuzzy shell that has a width $2\sigma_{ext}$ = (59 ± 1) nm. Therefore, the total size of the hollow microgel, in pure heavy water at *T* = (20.0 ± 0.5) °C and a concentration ζ = 0.08 ± 0.01, is R_{HS} = (190 ± 4) nm with a polydispersity σ_p = (13 ± 1)%. These values agree with the hydrodynamic radius and size polydispersity obtained by DLS: R_h = (211 ± 3) nm and *p* = (11 ± 4) %, respectively. As expected, the hydrodynamic radius is larger than the radius obtained from SANS since the latter is less sensitive to the polymeric dangling chains at the periphery of the microgel.[1,7,8,20,38]

Above the volume phase transition, at *T* = (40.0 ± 0.5) °C, the two fuzzy regions are completely deswollen and the cavity increases up to (47.0 ± 0.9) nm, solid red line in Fig. 3(b). The region with constant polymer density is compressed to a value *ws* = (36 ± 1) nm. The collapsed microgel has a total size R_{HS} = (83 ± 2) nm, equal to 56% of the radius in the swollen state. As expected, the cavity is conserved after core dissolution and is smaller than the original silica core. This is consistent with previous SANS measurements on similar systems.[7–9]

The cyan empty triangles in Fig. 3(a) represent the scattered intensity of the hollow microgels embedded within a matrix of regular deuterated ones. The total volume fraction, ζ, equals 1.04 ± 0.03 while the volume fraction of the hollow spheres in suspension is ζ_{HS} = 0.08 ± 0.01. A distinguishing feature of this curve with respect to the diluted case, both above and below the VPTT, is the absence of the shoulder in the low *q*-regime (see red empty squares at $3{\cdot}10^{-2}$ nm^{-1} < *q* < $5{\cdot}10^{-2}$ nm^{-1} and cyan empty circles at $6{\cdot}10^{-2}$ nm^{-1} < *q* < 10^{-1} nm^{-1}). Furthermore, compared to the swollen state, cyan empty circles, the concentrated sample shows a steeper decay of the form factor. These two observations are consistent with the collapse of the microgel and a change in its internal structure.[7–9]

The dashed-dotted line in Fig. 3(b) shows the relative polymer volume fraction within the microgel at ζ = 1.04 ± 0.03. The increase in concentration leads to a compression to a size comparable to the one of the collapsed microgels at (40.0 ± 0.5) °C. Nevertheless, the polymer distribution inside the microgel is different: Due to the overcrowded environment, the polymeric chains are pushed inside the cavity, which almost disappears. By contrast, an increase of the temperature conserves the cavity and strongly increases the polymer density within the microgel [solid red line in Fig. 3(b)].

This difference derives from the fact that when the temperature increases, the water (or heavy water) becomes a worse solvent for pNIPAM and, thus, the microgel tends to minimize its water content. By contrast, when the concentration of the suspension rises, the osmotic pressure outside the microgel is larger than inside.[20,28] Since there is no rigid core that opposes to the compression, the polymer tends to occupy the cavity. This response to overcrowded environments is a unique property of these microgels. For instance, other hollow architectures such as liposomes,[52] polyelectrolyte capsules,[53] or viruses[54] either deform or explode once external pressure is applied.

In Fig. 3(b), the dotted and dashed curves are drawn based on the results of the fit of the data, at (20.0 ± 0.5) °C, for concentrations at ζ = 0.244 ± 0.006 and ζ = 0.77 ± 0.02, respectively. The radial profile of the sample with ζ = 0.244 ± 0.006 is virtually identical to the one in the diluted condition, solid blue line. The radius of the cavity is R_{cav} = (36 ± 1) nm

and the total size of the microgel is R_{HS} = (187 ± 3) nm. In this case, the polydispersity is σ_p = (11 ± 2)%.

The sample at $\zeta = 0.77 \pm 0.02$ is smaller than the microgels at low concentrations. The parameters obtained from the fit of the data are: R_{cav} = (26 ± 1) nm, $2\sigma_{int}$ = (15 ± 2) nm, ws = (68 ± 2) nm, and $2\sigma_{ext}$ = (22 ± 1) nm. These values lead to a total radius R_{HS} = (131 ± 6) nm with a size polydispersity of σ_p = (13 ± 1)%. Interestingly, together with the deswelling of the microgel, the polymer already starts to penetrate into the void, leading to a decrease in R_{cav} with respect to the swollen state.

Figure 3(c) shows the total radius of the hollow microgel versus the generalized volume fraction (red empty circles). The values of R_{HS} are obtained from the fits of the data relative to the hollow microgels at different concentrations measured by SANS with contrast variation and shown in Fig. 3(a) and Figs. S4 and S5 of the supplementary material. The compression of the microgel starts at ζ = 0.55 ± 0.01, before direct contact between the microgels. This effect has been explained with the increase of the osmotic pressure of the suspension due to the contribution of the counter-ion clouds surrounding the microgels. Even for neutral microgels, charged groups originating from the initiator agent (e.g., ammonium persulfate or KPS) are incorporated at the periphery of the microgels.[55] Once these clouds percolate the available volume between the microgels, the ions contribute to the osmotic pressure of the suspensions. When the osmotic pressure of the suspension is comparable to the bulk modulus of the microgels, they deswell even before direct contact.[20]

For concentrations at ζ = 0.77 ± 0.02 and ζ = 1.04 ± 0.03, (dashed black line) and (dashed-dotted green line), however, the polymer is pushed inside the cavity. This shows how the contact between the microgels represents a second contribution to the compression that modifies the internal structure of the microgel. The polymeric chains rearrange within the cavity and the external fuzzy shell is completely collapsed once the microgels are further compressed. This effect can cause the second step in the compression, seen in Fig. 3(c) at $\zeta \geq 0.8$.

To verify that the hollow fuzzy-sphere model is not biasing the data fit due to the assumed architecture, a second model has been used to fit the experimental form factors and evaluate the radial profiles of the relative polymer volume fraction within the microgel. The multi-shell model used in Ref. 56 determines the radial profile corresponding to the best data fit, without any *a priori* assumption on the internal architecture of the microgel. This model divides the sphere in i-shells of the same lengths and then varies the relative polymer volume fraction of the ith shell to improve the data fit. At the end of the iterative fitting routine, the radial profile that produces the best fit of the scattering data is obtained.

As discussed in the supplementary material and shown in Fig. S4, the fit of the data with the two methods leads to virtually identical radial profiles for both low and high ζ. This proves on one hand that the assumption of a hollow structure is justified even for high ζ and on the other hand the reliability and robustness of the radial profile of the relative polymer volume fraction derived from the best fit of the data with the hollow fuzzy-sphere model.

For the samples with different concentrations, from $\zeta = 0.244 \pm 0.006$ up to $\zeta = 0.90 \pm 0.02$, all the other experimental form factors measured by SANS with contrast variation and the relative fits are shown in Figs. S4 and S5 of the supplementary material.

All the experimental scattering data can be fit with a hollow-sphere model. On one hand, the analysis of the data shows unambiguously that the cavity is conserved in all the ζ-range explored with SANS. On the other hand, deformations and deviations from the spherical shape might not be detectable with SANS due to both the size polydispersity of the microgels and the resolution of the instrument. An example of this comes from the icosahedral capsid of viruses, a clearly not spherical object that can be successfully fitted using a spherical core-shell model.[57] Furthermore, SANS experiments in a higher ζ-region were not possible due to unsuccessful redispersion of the microgels in the solvent. Neither cooling-heating loops nor long time stirring led to a homogeneous dispersion of the microgels in suspension.

Therefore, molecular dynamic simulations are performed to further investigate whether the hollow microgels embedded within a matrix of regular ones maintain the cavity at concentrations higher than the ones explored experimentally with SANS and whether they could be deformed for such high concentrations.

Computer simulations have already been used to successfully describe the swelling/deswelling of hollow shell and hollow double-shell microgels above and below the volume phase transitions, i.e., for bad and good quality of the solvent.[9,14,58] References 9, 14, and 58 simulated microgels with comparable cross-linking densities with respect to the microgels used in our manuscript and showed that the cavity persists upon collapse of the microgels, sometimes getting even larger than in the good solvent. Since simulations of diluted microgels are able to give an insight on the swelling/deswelling of the microgels below and above the VPTT, the same system has been used in this study to model the hollow microgels.

To reproduce the SANS experiments, a single hollow microgel was placed in the simulation box, surrounded by the regular microgels. The initial structure of the microgels ordered with the symmetry of the face-centered cubic (fcc) lattice is shown in Fig. 4(a). Here, for the clarity of demonstration of their mutual positions, only a part of the beads belonging to the sphere of radius $0.6R$ (R being the radius of the microgels) is visualized. The hollow microgel is depicted in red whereas all continuous microgels are in gray. The radial distribution function of the fcc structure is shown in Fig. 4(b).

The first concentration used in the computer simulations to study the effect of the neighbors compressing the hollow microgel was the one where the microgels were just in contact (overlap concentration or dense packing of the microgels swollen in a good solvent). The compression was achieved by decreasing the size of the simulation box. The maximum compression was achieved by reducing all linear sizes of the simulation box to half of the initial value.

The radial distribution of the polymer within the microgels can be computed directly from the results of the simulations. Figure 5(a) shows the evolution of the internal

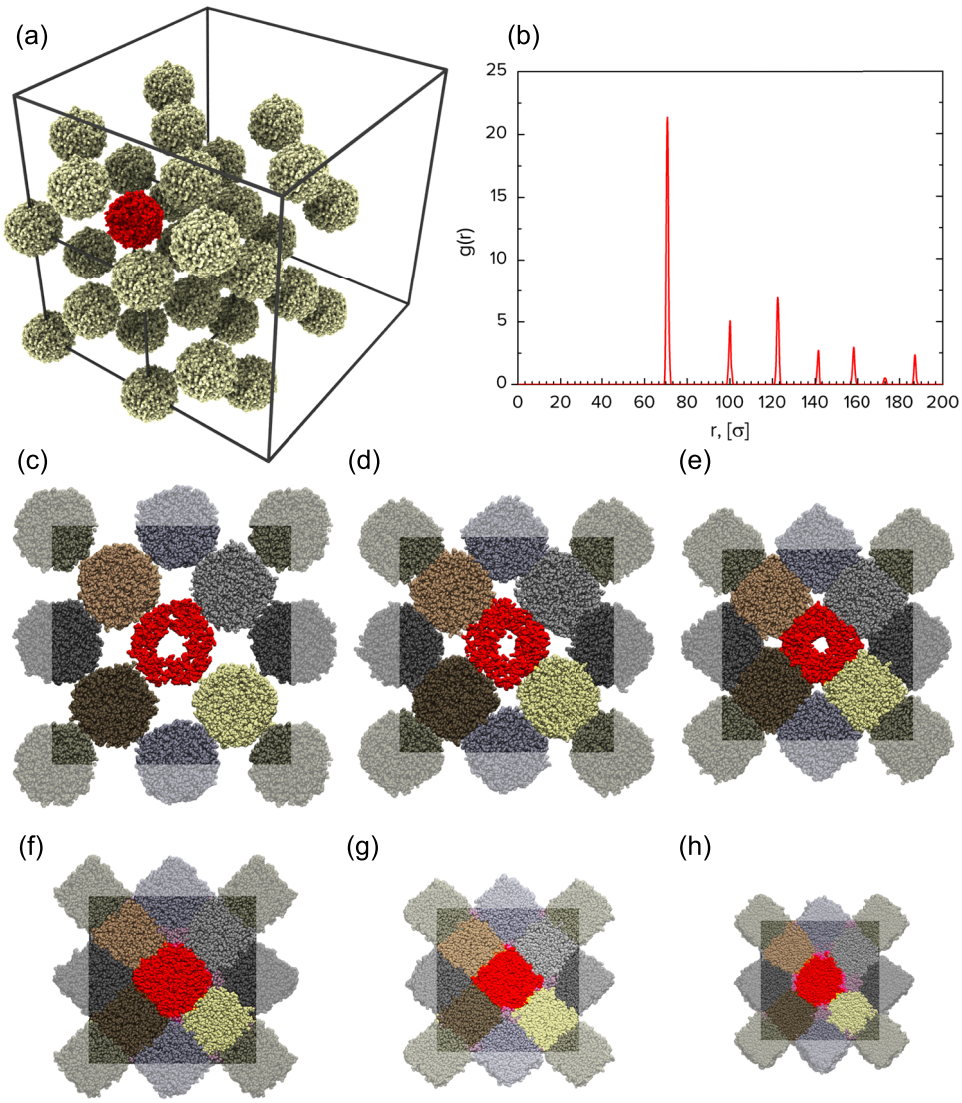

FIG. 4. (a) Initial positions of 32 microgel particles in a cubic simulation box of linear size $L_x = L_y = L_z = 200\sigma$. The elementary cell of the face-centered cubic lattice is shown as a small gray cube. Hollow microgel is depicted in red. (b) Radial distribution function of centers of mass of the microgels. Cross section of the simulation box through the center of mass of the hollow microgel (red) at different compression degree α: $\alpha = 1$ (c), 0.9 (d), 0.8 (e), 0.7 (f), 0.6 (g), and 0.5 (h). Continuous microgels are shown by different colors to demonstrate vanishingly weak interpenetration.

structure of the hollow microgel with increasing concentration. As soon as the microgels are compressed above the direct contact ($\alpha < 1$), the total size of the microgel decreases as shown by the blue and light blue curves. This decrease is accompanied by an increase of the polymer concentration in the shell and partial penetration of the polymer into the cavity (the cavity size decreases). On the other hand, the shell thickness does not change considerably upon compression.

With decreasing box size (i.e., increasing microgel concentration), a further deswelling produces a strong expansion of the polymer into the cavity. The first three curves in Fig. 5(a) (blue, light blue, and black) are in excellent agreement with the radial profiles obtained form the fit of the experimental data shown in Fig. 3(b). Nevertheless, the simulations predict the persistence of external fuzziness, in contrast to SANS. This discrepancy can be explained with the fact that a constant distribution of cross-linker through the microgel is assumed in computer simulations. Such a uniformly cross-linked polymer network can underestimate the capability of the periphery to get compressed more easily than the internal, more cross-linked region with constant polymer density and, in general, affect the mechanical response of the simulated microgels.[59] Despite these differences, connected to the simplified model used to reproduce the microgels in the simulations, the qualitative agreement of the trends of the polymer volume fraction with the ones obtained from SANS shows that the presence of the cavity persists for low compressions and confers to the hollow microgels a unique opportunity to respond to overcrowded environments, unobserved in other colloidal systems.

A further decrease of the box sizes, $\alpha \leq 0.7$, allows us to quantitatively estimate the response of the hollow microgels at high concentrations, not probed experimentally. As shown by the profiles in Fig. 5(a), the cavity is completely occupied by the polymer chains and the fuzziness of the microgels strongly decreases from the pink curve ($\alpha = 0.7$) to the orange profile ($\alpha = 0.5$). This indicates that for very high concentrations, the hollow microgels are further compressed and this leads the polymer chains to rearrange and completely occupy the cavity. Again, the architecture of the microgels might be slightly different than the profiles shown in Fig. 5(a), e.g., the fuzziness might disappear at lower

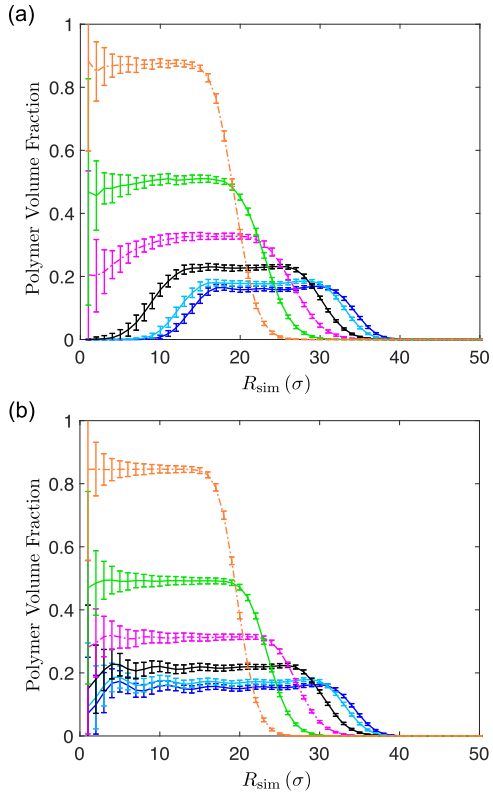

FIG. 5. Polymer volume fraction as obtained from the computer simulations within the hollow (a) and regular (b) microgel as a function of radial coordinate R_{sim} measured in units of the bead radius σ at different compression degrees, α. Bottom to top: α = 1, 0.9, 0.8, 0.7, 0.6, and 0.5.

concentrations. This is due to the inhomogeneous distribution of cross-linker that is not considered in computer simulations. Nevertheless, the key point confirmed by these simulations is that the cavity does not compromise the mechanical stability of the hollow microgels once they are strongly squeezed by their neighbors.

In contrast to SANS with contrast matching where the matrix of the regular microgels is not visible, computer simulations can probe the behavior of the regular microgels together with the shape of the hollow microgels. Figure 5(b) shows the radial density profiles of the regular microgels. They have nearly the same polymer volume fraction as hollow microgels at the corresponding compression degrees. This means that the different microgels are in equilibrium with each other under any compression degree. Figures 4(c)–4(h) show the cross section of the simulation box through the center of mass of the hollow microgel. The hollow microgel is reported in red surrounded by the regular ones with different colors. These images offer the possibility to evaluate both how spherical the hollow microgels are at different compressions and the behavior of the regular microgels composing the matrix.

Figures 4(c) and 4(d) represent the first stages of the compression where it is evident that the microgels, both hollow and regular, do not significantly deviate from the spherical shape. The reduction of the cavity, occupied by the polymer, appears clear as well. Deviation from a sphere appears in Fig. 4(e) and becomes more and more dramatic in the panels in the third row of Fig. 4. This effect is driven by homogenization of the system upon compression: All solvent-rich interstitial space between the microgels is filled by the polymer. The fcc-ordering of the microgels is retained upon compression with sufficient accuracy, Figs. 4 and S9 of the supplementary material, due to a small difference in masses of the hollow and regular microgels. In other words, the "impurity" caused by the hollow microgels with lower molecular weight is not enough to induce essential defects of the crystalline structure. Therefore, each microgel practically adopts the shape of the Wigner-Seitz cell, represented by the rhombic dodecahedron shown in Fig. 6. Deviations from the ideal structure highlighted by the beads outside the cell and by "empty" spaces inside (they are occupied by beads from the neighboring microgels) are pretty small.

Comparable faceting of microgels has been observed using both confocal-[22] and super resolved-microscopy[23] for regular larger microgels at higher concentrations than the ones used for the experimental study of this work. The fact that at high concentrations the deformations are shown in computer simulations, but not with SANS, can have a double explanation. First, such deformations produce minimal effects on the scattering profiles that are further attenuated by both the instrument resolution and the sample polydispersity making it impossible to distinguish a sphere from an object inscribed within the Wigner-Seitz cell. Second, the concentrations, where computer simulations detect the deformations, are well above the concentrations measured in our experiments.

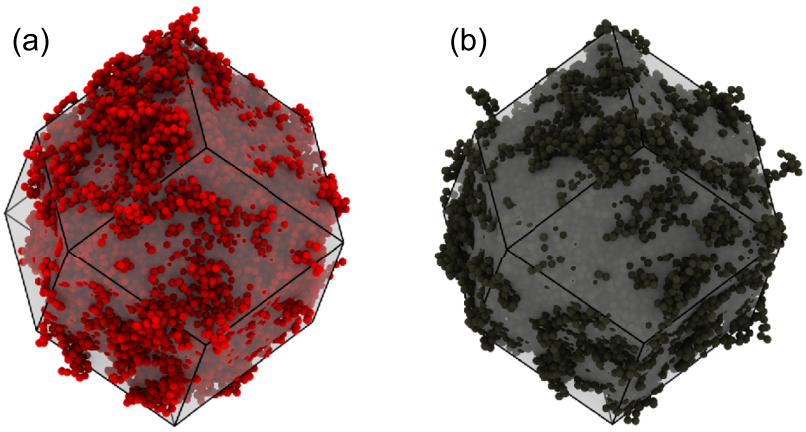

FIG. 6. Typical structures of hollow (a) and continuous (b) microgels under the condition of maximum compression, α = 0.5. The Wigner-Seitz cell of the fcc structure is shown by the semitransparent rhombic dodecahedron. The beads, which are outside the Wigner-Seitz cell, and "empty" spaces inside can be attributed to defects of the crystalline structure.

IV. CONCLUSIONS

We have presented the first detailed experimental description of the behavior of hollow microgels embedded in overcrowded environments. SANS with contrast matching shows that the microgels are compressed while maintaining their spherical shape. No deformations, such as buckling or failure, are observed. For low concentrations, these findings are strongly supported by computer simulations. Thus, the absence of a rigid core does not prejudice the structural stability of the hollow microgels once these are squeezed by their neighbors.

For very high concentrations, probed only with computer simulations, initial fcc-ordering retains due to the small difference in masses of the hollow and regular microgels. Herewith, the shape of the microgels transforms into the shape of the Wigner-Seitz cell. These findings agree with recent work where faceting of large microgels was observed in overcrowded environments with microscopy techniques.[22,23]

Both experiments and computer simulation show that the empty cavity allows for an alternative mechanism to respond to the compression: The polymer chains are pushed and rearrange within the cavity. By contrast, regular microgels can adapt to the squeeze only by deswelling[20] or interpenetrating each other.[21]

Recent studies have shown that differences between the bulk moduli of the microgels involved in a mixture lead the softer ones to deswell first.[49] A decrease of the size of ≈20% was reached at a volume fraction similar to the ones experimentally probed in the presented study.[20] By contrast, when the elasticities of the polymer networks are very close, interpenetration between them looks to be the predominant response to the overcrowded environment, without a significant decrease of the size of the microgels in suspension.[21]

In our work, hollow microgels have been synthesized with the same amount of cross-linker used for the deuterated regular microgels of the matrix, 5 mol. % of BIS. Therefore, the stiffnesses of the polymer networks of the hollow and regular microgels are comparable. In this case, according to the literature, interpenetration is expected to be dominant with respect to deswelling.[21,47] By contrast, we observed the deswelling of the hollow microgels that is even more pronounced with respect to the case of mixing regular microgels with a mismatch between their bulk moduli.[20,60] Our results show that the presence of a cavity within the microgel has a strong effect on its deswelling, leading to a size decrease of ≈56%.

If we define as "softness" the capability of the microgels to reduce their size in overcrowded environments, the hollow microgels are softer than regular microgels synthesized with the same amount of cross-links. Furthermore, the internal cavity produces a more pronounced deswelling with respect to the case shown in Ref. 20. These two considerations lead to the conclusion that a cavity has a strong impact on the deswelling of the hollow microgels making them substantially different and softer than the regular counterpart.

Recently, we have also shown that hollow microgels adsorbed on a solid substrate maintain their cavity.[61] From the present study, it is evident that hollow microgels conserve the cavity even at high concentrations, in overcrowded environments. These two results suggest that hollow microgels adsorbed on a solid interface remain hollow independently on the concentrations. These facts candidate the hollow microgels as a key system to develop either coatings that enable cell invasion within restrictive fibrillar polymers[62] or thermoresponsive membranes for separation, synthesis, and catalytic applications.[13,63]

SUPPLEMENTARY MATERIAL

See supplementary material for dynamic light scattering and viscosimetry characterization of the microgels. Furthermore, additional SANS data fit and the experimental determination of the match point for the deuterated microgels are included. A section regarding the computer simulation is included as well. Experimental data for these articles are available under request at https://hdl.handle.net/21.11102/3fc4ed1a-10cb-11e8-80f7-e41f1366df48.

ACKNOWLEDGMENTS

A.S. thanks the Alexander von Humboldt Foundation for the financial support. Financial support from No. SFB 985 "Functional Microgels and Microgel Systems" of Deutsche Forschungsgemeinschaft within Project A3 and from the International Helmholtz Research School of Biophysics and Soft Matter (IHRS BioSoft) is greatly acknowledged. This work was supported by the Russian Science Foundation, Project No. 15-13-00124. The authors gratefully acknowledge the computing time granted by the John von Neumann Institute for Computing (NIC) and provided on the supercomputer JURECA[64] at the Jülich Supercomputing Centre (JSC). This work is based upon experiments performed at the KWS2 instrument operated by JCNS at the Heinz Maier-Leibnitz Zentrum (MLZ), Garching, Germany.

[1] M. Stieger, W. Richtering, J. Pedersen, and P. Lindner, J. Chem. Phys. **120**, 6197 (2004).
[2] N. Hatto, T. Cosgrove, and M. Snowden, Polymer **41**, 7133 (2000).
[3] M. Karg, I. Pastoriza-Santos, L. M. Liz-Marzán, and T. Hellweg, ChemPhysChem **7**, 2298 (2006).
[4] M. Karg, S. Wellert, S. Prevost, R. Schweins, C. Dewhurst, L. M. Liz-Marzán, and T. Hellweg, Colloid Polym. Sci. **289**, 699 (2011).
[5] S. Nayak, D. Gan, M. Serpe, and L. Lyon, Small **1**, 416 (2005).
[6] V. Lapeyre, N. Renaudie, J.-F. Dechezelles, H. Saadaoui, S. Ravaine, and V. Ravaine, Langmuir **25**, 4659 (2009).
[7] J. Dubbert, T. Honold, J. S. Pedersen, A. Radulescu, M. Drechsler, M. Krag, and W. Richtering, Macromolecules **47**, 8700 (2014).
[8] J. Dubbert, K. Nothdurft, M. Krag, and W. Richtering, Macromol. Rapid Commun. **36**, 159 (2015).
[9] A. J. Schmid, J. Dubbert, A. A. Rudov, J. S. Pedersen, P. Lindner, M. Karg, I. I. Potemkin, and W. Richtering, Sci. Rep. **6**, 22736 (2016).
[10] Z. Xing, C. Wang, J. Yan, L. Zhang, L. Li, and L. Zha, Soft Matter **7**, 7992 (2011).
[11] H. Masoud and A. Alexeev, ACS Nano **6**, 212 (2012).
[12] G. Liu, C. Zhu, J. Xu, Y. Xin, T. Yang, J. Li, L. Shi, Z. Guoa, and W. Liu, Colloids Surf., B **111**, 7 (2013).
[13] B. P. Tripathi, N. C. Dubey, and M. Stamm, ACS Appl. Mater. Interfaces **6**, 17702 (2014).

[14]K. Geisel, A. A. Rudov, I. I. Potemkin, and W. Richtering, Langmuir **31**, 13145 (2015).
[15]L. Zha, Y. Zhang, W. Yang, and S. Fu, Adv. Mater. **14**, 1090 (2002).
[16]F. A. Plamper and W. Richtering, Acc. Chem. Res. **50**, 131 (2017).
[17]U. Gasser, J.-J. Lietor-Santos, A. Scotti, O. Bunk, A. Menzel, and A. Fernandez-Nieves, Phys. Rev. E **88**, 052308 (2013).
[18]M. Pelaez-Fernandez, A. Souslov, L. A. Lyon, P. M. Goldbart, and A. Fernandez-Nieves, Phys. Rev. Lett. **114**, 098303 (2015).
[19]J. Ruiz-Franco, J. Marakis, N. Gnan, J. Kohlbrecher, M. Gauthier, M. P. Lettinga, D. Vlassopoulos, and E. Zaccarelli, Phys. Rev. Lett. **120**, 078003 (2018).
[20]A. Scotti, U. Gasser, E. S. Herman, M. Pelaez-Fernandez, L. A. Lyon, and A. Fernandez-Nieves, Proc. Natl. Acad. Sci. U. S. A. **113**, 5576 (2016).
[21]P. S. Mohanty, S. Nöjd, K. v. Gruijthuijsen, J. J. Crassous, M. Obiols-Rabasa, R. Schweins, A. Stradner, and P. Schurtenberger, Sci. Rep. **7**, 1487 (2017).
[22]I. Bouhid de Aguiar, T. van de Laar, M. Meireles, A. Bouchoux, J. Sprakel, and K. Schroën, Sci. Rep. **7**, 10223 (2017).
[23]G. M. Conley, P. Aebischer, S. Nöjd, P. Schurtenberger, and F. Scheffold, Sci. Adv. **3**, e1700969 (2017).
[24]C. N. Likos, H. Löwen, M. Watzlawek, B. Abbas, O. Jucknischke, J. Allgaier, and D. Richter, Phys. Rev. Lett. **80**, 4450 (1998).
[25]P. N. Pusey and W. van Megen, Nature **320**, 340 (1986).
[26]D. Paloli, P. S. Mohanty, J. J. Crassous, E. Zaccarelli, and P. Schurtenberger, Soft Matter **9**, 3000 (2013).
[27]V. Chikkadi, D. M. Miedema, M. T. Dang, B. Nienhuis, and P. Schall, Phys. Rev. Lett. **113**, 208301 (2014).
[28]P. van der Scheer, T. van de Laar, J. van der Gucht, D. Vlassopoulos, and J. Sprakel, ACS Nano **11**, 6755 (2017).
[29]W. Stöber, A. Fink, and E. Bohn, J. Colloid Interface Sci. **26**, 62 (1968).
[30]M. Andersson and S. L. Maunu, J. Polym. Sci., Part B: Polym. Phys. **44**, 3305 (2006).
[31]H. Shirota and K. Horie, Chem. Phys. **242**, 115 (1998).
[32]H. Shirota, N. Kwabara, K. Ohkawa, and K. Horie, J. Phys. Chem. B **103**, 10400 (1999).
[33]D. E. Koppel, J. Chem. Phys. **57**, 4814 (1972).
[34]W. Burchard and W. Richtering, Prog. Colloid Polym. Sci. **80**, 151 (1989).
[35]R. C. Hardy and R. L. Cottington, J. Res. Natl. Bur. Stand. **42**, 573 (1949).
[36]S. W. Provencher, Makromol. Chem. **180**, 201 (1979).
[37]S. W. Provencher, Comput. Phys. Commun. **27**, 213 (1982).
[38]A. Scotti, W. Liu, J. S. Hyatt, E. S. Herman, H. S. Choi, J. Kim, L. A. Lyon, U. Gasser, and A. Fernandez-Nieves, J. Chem. Phys. **142**, 234905 (2015).
[39]M. Shibayama, T. Tanaka, and C. C. Han, J. Chem. Phys. **97**, 6829 (1992).
[40]A. M. Rumyantsev, A. A. Rudov, and I. I. Potemkin, J. Chem. Phys. **142**, 171105 (2015).
[41]R. Schroeder, A. A. Rudov, L. A. Lyon, W. Richtering, A. Pich, and I. I. Potemkin, Macromolecules **48**, 5914 (2015).
[42]S. Plimpton, J. Comput. Phys. **117**, 1 (1995).
[43]K. Kremer and G. Grest, J. Chem. Phys. **94**, 4103 (1991).
[44]S. Toxvaerd and J. C. Dyre, J. Chem. Phys. **134**, 081102 (2011).
[45]P. J. Daivis and B. D. Todd, J. Chem. Phys. **124**, 194103 (2006).
[46]D. J. Evans and G. P. Morriss, Phys. Rev. A **30**, 1528 (1984).
[47]U. Gasser, J. Hyatt, J.-J. Lietor-Santos, E. Herman, L. Lyon, and A. Fernandez-Nieves, J. Chem. Phys. **141**, 034901 (2014).
[48]P. Voudouris, D. Florea, P. van der Schootbc, and H. Wyss, Soft Matter **9**, 7158 (2013).
[49]A. S. J. Iyer and L. A. Lyon, Angew. Chem., Int. Ed. **48**, 4562 (2009).
[50]M. Stieger, J. S. Pedersen, P. Lindner, and W. Richtering, Langmuir **20**, 7283 (2004).
[51]P. S. Pedersen, D. Posselt, and K. Mortensen, J. Appl. Crystallogr. **23**, 321 (1990).
[52]A. Yaroslavov, I. Panova, A. Sybachin, V. Spiridonov, A. Zezin, O. Mergel, A. Gelissen, R. Tiwari, F. Plamper, W. Richtering, and F. Menger, Nanomed.: Nanotechnol., Biol. Med. **13**, 1491 (2017).
[53]C. Gao, E. Donath, S. Moya, V. Dudnik, and H. Möhwald, Eur. Phys. J. E **5**, 21 (2001).
[54]G. A. Vliegenthart and G. Gompper, Biophys. J. **91**, 834 (2006).
[55]J. Zhou, J. Wei, T. Ngai, L. Wang, D. Zhu, and J. Shen, Macromolecules **45**, 6158 (2012).
[56]O. L. J. Virtanen, A. Mourran, P. T. Pinard, and W. Richtering, Soft Matter **12**, 3919 (2016).
[57]D. A. Kuzmanovic, I. Elashvili, C. Wick, C. O'Connell, and S. Krueger, Structure **11**, 1339 (2003).
[58]M. Brugnoni, A. Scotti, A. A. Rudov, A. P. H. Gelissen, T. Caumanns, A. Radulescu, T. Eckert, A. Pich, I. I. Potemkin, and W. Richtering, Macromolecules **51**, 2662 (2018).
[59]N. Gnan, L. Rovigatti, M. Bergman, and E. Zaccarelli, Macromolecules **50**, 8777 (2017).
[60]A. Scotti, U. Gasser, E. S. Herman, J. Han, A. Menzel, L. A. Lyon, and A. Fernandez-Nieves, Phys. Rev. E **96**, 032609 (2017).
[61]M. F. Schulte, A. Scotti, A. P. H. Gelissen, W. Richtering, and A. Mourran, Langmuir **34**, 4150 (2018).
[62]A. M. Douglas, A. A. Fragkopoulos, M. K. Gainesa, L. A. Lyon, A. Fernandez-Nieves, and T. H. Barker, Proc. Natl. Acad. Sci. U. S. A. **114**, 885 (2015).
[63]D. Menne, F. Pitsch, J. E. Wong, A. Pich, and M. Wessling, Angew. Chem., Int. Ed. **53**, 5706 (2014).
[64]D. Krause and P. Thörnig, "JURECA: General-purpose supercomputer at Jülich Supercomputing Centre," J. Large-Scale Res. Facil. **2**, A62 (2016).